Magnetic properties of nanomagnetic and biomagnetic systems analyzed using cantilever magnetometry

2011 Nanotechnology 22 285715

(http://iopscience.iop.org/0957-4484/22/28/285715)

Nanotechnology **22** (2011) 285715 (8pp) doi:10.1088/0957-4484/22/28/285715

Magnetic properties of nanomagnetic and biomagnetic systems analyzed using cantilever magnetometry

Urs Gysin[1], Simon Rast[2], Andreas Aste[3], Thanassis Speliotis[4], Christoph Werle[1] and Ernst Meyer[1]

[1] Department of Physics, University of Basel, Klingelbergstrasse 82, 4056 Basel, Switzerland
[2] Steinrebenstrasse 43, CH-4153 Reinach, Switzerland
[3] Paul Scherrer Institut (PSI), CH-5232 Villigen PSI, Switzerland
[4] Institute of Materials Science, NCSR Demokritos, Aghia Paraskevi, Attika, Athens 15310, Greece

E-mail: urs.gysin@unibas.ch

Received 7 March 2011, in final form 18 May 2011
Published 9 June 2011
Online at stacks.iop.org/Nano/22/285715

Abstract
Magnetic properties of nanomagnetic and biomagnetic systems are investigated using cantilever magnetometry. In the presence of a magnetic field, magnetic films or particles deposited at the free end of a cantilever give rise to a torque on the mechanical sensor, which leads to frequency shifts depending on the applied magnetic field. From the frequency response, the magnetic properties of a magnetic sample are obtained. The magnetic field dependences of paramagnetic and ferromagnetic thin films and particles are measured in a temperature range of 5–320 K at a pressure below 10^{-6} mbar. We present magnetic properties of the ferromagnetic materials Fe, Co and Ni at room temperature and also for the rare earth elements Gd, Dy and Tb at various temperatures. In addition, the magnetic moments of magnetotactic bacteria are measured under vacuum conditions at room temperature. Cantilever magnetometry is a highly sensitive tool for characterizing systems with small magnetic moments. By reducing the cantilever dimensions the sensitivity can be increased by an order of magnitude.

(Some figures in this article are in colour only in the electronic version)

1. Introduction

The knowledge of the magnetic properties of nanoscale structures is of fundamental interest and necessary for the development of future technical applications in ferromagnetism [1], magnetic recording media [2], spin electronics [3] and biomedicine [4].

The magnetic phenomena on the microscale and nanoscale can strongly deviate from those of macroscale phenomena. Theory and experiments may differ by an order of magnitude in micromagnetic systems, such as that of Brown's paradox [5].

Micromechanical cantilevers used in atomic force microscopy [6] (AFM) are highly sensitive force and torque sensors and therefore ideal tools for detecting magnetic properties of small samples. The torque acting on the magnetic system placed at the free end of a cantilever results in a change of the eigenfrequency of a self-oscillating cantilever depending on the applied magnetic field. The magnetic properties are derived from the frequency response versus magnetic field curve (f–H curve). The dimensions of the cantilever and the frequency noise determine the detection sensitivity.

The different types of magnetism are discerned from the shape of the magnetic moment versus field curve (m–H curve). A linear relation between the magnetic moment and magnetic field is found for paramagnetic samples. For ferromagnetic samples the m–H curve shows hysteresis in the easy axis direction. The coercive field H_c, the remanence field B_r and the saturation field can be obtained from the m–H curve.

In this paper we discuss the characteristics of f–H curves obtained by cantilever magnetometry [7–10] for paramagnetic, soft and hard ferromagnetic systems. From the shape of the frequency response curve the different types of magnetism

are distinguished. Furthermore, magnetic properties of magnetotactic bacteria (*Magnetospirillum gryphiswaldense bacteria*) are investigated.

A theoretical model based on Stoner and Wohlfarth's [11] ideas is developed to determine the magnetic properties of ferromagnetic samples.

Compared to other magnetic analyzing techniques based on micromechanical cantilevers, for instance magnetic force microscopy [12, 13] (MFM), where the stray field above the magnetic sample is analyzed, cantilever magnetometry measures the magnetic moment of the entire magnetic sample placed at the free end of the cantilever.

2. Theory

Cantilever magnetometry measures the eigenfrequency of a self-oscillating cantilever depending on an external magnetic field $\vec{H}_{\text{ext}}$. Due to the electromagnetic interaction between the external field and the magnetic moment of the system placed at the free end of the cantilever, the eigenfrequency changes on varying the external field. From such frequency shift curves (f–H curves) the magnetic properties are determined.

2.1. Paramagnetic particles

The advantage of using a paramagnetic sample is that we know how the magnetization $\vec{M}$ will behave, depending on an external applied field $\vec{H}_{\text{ext}}$. The magnetization $\vec{M} = \chi \vec{H}_{\text{int}}$ of the particle is a linear function of the internal magnetic field $\vec{H}_{\text{int}}$. The scalar factor χ is the volume susceptibility of the paramagnetic material. The corresponding magnetic moment is $\vec{m} = \vec{M}V$, where V is the volume of the paramagnetic particle.

The internal field $\vec{H}_{\text{int}}$ of an ellipsoidal magnetic particle is reduced by its demagnetization field[5] [14] $\vec{H}_{\text{int}} = \vec{H}_{\text{ext}} - (\hat{S}\hat{N}\hat{S}^{-1})\vec{M}$. The demagnetization tensor $\hat{N}$, solely depending on the geometry of the particle, is diagonalized for an ellipsoidal particle in the oscillating cantilever system in the case where the coordinate axes are parallel to the axes of the ellipsoid. The diagonal elements are N_x, N_y and N_z. We have to transform the tensor into the static laboratory system with the rotation matrix $\hat{S}$ for a deflection angle β of the cantilever due to the oscillation (see figure 1) around the x-axis. For small cantilever amplitudes z, typically smaller than 1 μm, the angle of deflection is approximated by $\beta = z/\tilde{L}$. The reduced length $\tilde{L} = L/\alpha$ is the cantilever length L divided by a factor $\alpha = 1.377$ for the first eigenmode [15].

With these relations we can calculate the magnetization $\vec{M} = (\chi^{-1} + (\hat{S}\hat{N}\hat{S}^{-1}))^{-1}\vec{H}_{\text{ext}}$ for a paramagnetic particle. The torque acting on the magnetic particle is $\vec{\tau} = \mu_0 V(\vec{M} \times \vec{H}_{\text{ext}})$, where μ_0 is the magnetic field constant. For small torques, i.e. magnetic moments, typically less than 10^{-12} A m^2 for soft cantilevers, the free end of the cantilever does not twist and we assume that the same torque is acting on the hinge of the cantilever. The force acting on the particle equivalent to the torque mentioned above is $F = |\vec{\tau}|/\tilde{L}$.

[5] Calculation is in the SI system.

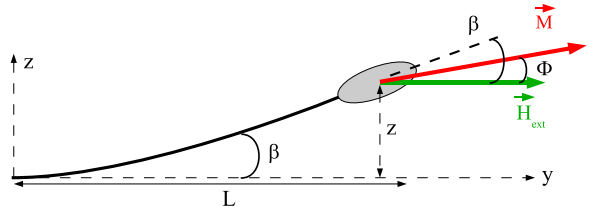

Figure 1. Schematic view of a cantilever with an ellipsoidal magnetic particle mounted at the free end of the cantilever. The external field $\vec{H}_{\text{ext}}$ is applied parallel to the cantilever hinge. $\vec{M}$ is the magnetization of the sample and ϕ is the angle between the magnetization $\vec{M}$ and the field $\vec{H}_{\text{ext}}$. The angle of the cantilever deflection β, caused by cantilever oscillation, is approximately $z/\tilde{L}$ for small cantilever amplitudes z, where $\tilde{L} = L/1.377$ is the reduced cantilever length and L the cantilever length.

For small changes in frequency and neglecting the particle mass, the frequency shift is $\Delta f = (f_0 \cdot k_{\text{mag}})/(2 \cdot k_0)$, where f_0 is the eigenfrequency of the cantilever in zero field, k_0 the zero-field spring constant and $k_{\text{mag}} = \partial F/\partial z$ is the additional spring constant caused by the interaction between the magnetic field and the magnetic particle. The expression for the frequency shift is valid under the assumption that $k_0 \gg k_{\text{mag}}$, which is well fulfilled in our case.

The force is expanded in a Taylor series for small cantilever amplitudes. For an ellipsoidal paramagnetic particle the frequency response becomes

$$\Delta f = \frac{1}{2}\frac{f_0 \mu_0 H_{\text{ext}}^2 V}{k_0 \tilde{L}^2} \cdot \frac{\chi^2 (N_z - N_y)}{1 + \chi(N_y + N_z) + \chi^2 N_y N_z}. \quad (1)$$

For an infinite magnetic layer the only non-vanishing element of the demagnetization tensor is perpendicular to the layer plane [14, 16, 17], i.e. $N_x = N_y = 0$ and $N_z = 1$; hence a frequency response is expected. On the other hand no frequency shift occurs for a paramagnetic sphere, where all three elements are equal: $N_x = N_y = N_z = \frac{1}{3}$. For a paramagnetic particle the shape of the particle is crucial for the behavior of the frequency response to the applied field.

Keeping in mind that for the experimentalist it will not be possible to mount the cantilever precisely parallel to the external field and furthermore the angle β due to oscillation is very small, actually much smaller than the misalignment, we therefore performed the same calculation at a magnetic field applied at an angle θ to the cantilever hinge. The correction is a factor $\cos(2 \cdot \theta)$ in equation (1) and does not influence the result significantly for a small misalignment angle θ. The cantilever is aligned with the magnetic field with an accuracy of about 2°.

2.2. Ferromagnetic particles

Hysteresis in ferromagnetism is the change of the entire magnetic moment of a domain ensemble depending on the external magnetic field. Three processes contribute to the hysteresis: the variation of the volume (e.g. domain wall motion), the change of the magnitude of the magnetization and the change of the orientation relative to the external magnetic field of each single domain.

Table 1. Magnetic sensitivity of three different cantilevers for a magnetic sphere in an external field of 1 T and with a 1 Hz measurement bandwidth. Cantilever 1 is commercially available, cantilever 2 is custom designed [22, 23] and cantilever 3 is a hypothetical cantilever for a sensitivity of 100 μ_B (Bohr magnetons).

	Cantilever 1	Cantilever 2	Cantilever 3
Frequency f_0 (Hz)	20×10^3	10×10^3	275×10^3
Length L (μm)	250	150	5
Width w (μm)	35	4	0.5
Thickness t (μm)	1	0.18	0.05
Spring constant k_0 (N m^{-1})	0.08	0.2×10^{-3}	3×10^{-3}
Temperature T (K)	293	5	5
Oscillation amplitude A (nm)	100	500	50
Quality factor (at 10^{-6} mbar)	10^5	10^5	10^5
Frequency noise δf (mHz)	0.6	0.2	3.4
Magnetic sensitivity (μ_B)	10^7	10^4	10^2

To calculate the magnetization in equilibrium we have to find the angle ϕ_{min} between the entire magnetization $\vec{M}$ and the external applied field $\vec{H}_{ext}$ by minimizing the total free energy [14] $\tilde{F} = \int (\tilde{F}_0 - \frac{1}{2}\mu_0 \vec{M}(\vec{H}_{int} + \vec{H}_{ext}))\,dV$ of the magnetic particle in the external magnetic field. Note that the expression for the free energy is only valid for particles with uniaxial anisotropy that are single domain, which is the case for a magnetic system in saturation. Thermodynamics requires for isothermal and isochoric processes that the free energy has a minimum in the thermal equilibrium. $\tilde{F}_0$ describes all anisotropies in addition to the shape anisotropy. Stoner and Wohlfarth [11] attest that the equilibrium magnetization lies in the plane, clamped by the external field and the spheroid polar axis. Therefore we can express the magnetization as $\vec{M}(\phi) = (0, M\cos(\phi), M\sin(\phi))$.

All additional anisotropies, e.g. crystalline anisotropy, are approximated with $\tilde{F}_0 = KV\sin^2(\beta - \phi)$, where K is the anisotropy constant [11, 18].

The free energy is differentiated with respect to the angle ϕ between the magnetization and external field and expanded in a Taylor series for small cantilever oscillation amplitude z and small angle ϕ and then set to zero in order to find the angle ϕ_{min} minimizing the free energy $\tilde{F}$.

With the knowledge of ϕ_{min} and the corresponding magnetization in equilibrium we calculate the torque $\vec{\tau} = \mu_0 V(\vec{M}(\phi_{min}) \times \vec{H}_{ext})$ acting on the ferromagnetic particle. The same procedures as for the paramagnetic ellipsoidal particle yield the frequency response for the cantilever depending on the external field

$$\Delta f = \frac{1}{2}\frac{f_0 \mu_0 H_{ext} V M}{k_0 \tilde{L}^2} \cdot \frac{\mu_0 M^2 (N_z - N_y) + 2K}{\mu_0 M H_{ext} + \mu_0 M^2 (N_z - N_y) + 2K}. \quad (2)$$

Again the same calculation for a field applied at an angle θ between cantilever hinge and field direction is arranged and exhibits a rather complicated correction to second-order θ. However for small misalignment, the result is not influenced strongly.

Furthermore the magnetic sensitivity of cantilever magnetometry depends on the dimensions of the cantilever. The quotient $f_0/(k_0\tilde{L}^2)$ has to be optimized to get a maximal frequency response. For a rectangular cantilever with length L, width w and thickness t, the sensitivity is proportional to $f_0/(k_0\tilde{L}^2) \propto (Lwt^2)^{-1}$. Reducing the dimensions, in particular the thickness, will increase the sensitivity.

On the other hand, the thermal frequency noise [19–21] $\delta f = \sqrt{f_0 k_B T B/(\pi k_0 Q A^2)}$ of the cantilever limits the sensitivity. Here, k_B is the Boltzmann constant, B the measurement bandwidth, Q the quality factor, A the oscillation amplitude and T the temperature of the cantilever.

For a magnetic sphere we can calculate the magnetic moment of the sphere from equation (2) and estimate the minimal detectable magnetic moment m_{min}. In table 1 the magnetic sensitivities for three kinds of cantilevers are calculated at 1 T, with a measurement bandwidth of 1 Hz. Cantilever[6] 1 is commercially available and it is possible to detect magnetic moments of 10^7 μ_B (Bohr magnetons) at room temperature. The sensitivity limit for the highly sensitive, custom designed cantilever [22, 23] (cantilever 2) at low temperature is about 10^4 μ_B (Bohr magnetons). By further reducing the dimensions, the sensitivity is increased and samples of about 100 μ_B may be investigated with a hypothetical cantilever 3 at low temperature.

3. The experimental method

The cantilever with the magnetic system is driven using a piezo-actuator at one of the flexural eigenmodes, typically the first. The frequency response of the cantilever depending on the applied magnetic field is demodulated with a fully digitized phase lock loop (PLL) electronic circuit [24]. The frequency resolution of the PLL is in the sub-microhertz regime, necessary for a magnetic resolution of 10^4 μ_B with current cantilevers (cantilever 2 in table 1). The demodulation bandwidth of the PLL is 0.1–1 Hz for sub-microhertz frequency resolution.

The measurements are performed in two different magnet systems. For experiments at low cantilever temperatures down to 5 K and magnetic fields up to ±7 T we use a superconducting magnet incorporated in an ultrahigh vacuum (UHV) cryostat [25]. The UHV system allows us to prepare and transfer the cantilevers into the superconducting magnet under UHV conditions.

[6] MikroMasch, CSC12, www.spmtips.com.

Another magnetometer is operated in an electromagnet[7] and provides a magnetic field up to ±1.3 T in the temperature range of 77–320 K. The cantilever is mounted in a small glass tube, which is located between the magnet poles of the electromagnet. A cooling finger filled with liquid nitrogen allows us to cool the cantilever. The tube is evacuated to a pressure below 10^{-6} mbar. Cantilever oscillations are measured using a beam deflection technique [26].

4. Results and discussion

Cantilever magnetometry is performed with different magnetic systems at temperatures ranging from 5 to 320 K. Metallic magnetic layer systems ranging from 2.5 to 40 nm in thickness are deposited at the free ends of commercial soft cantilevers by evaporation and sputtering techniques.

The magnetic moment for the rare earth elements gadolinium (Gd), terbium (Tb) and dysprosium (Dy) is caused by the electrons in the 4f shell. Dy and Tb are paramagnetic at room temperature, antiferromagnetic below room temperature and ferromagnetic at the temperature of liquid nitrogen (77 K) and below. The Curie and Néel temperatures of Dy are 85 K and 178 K [27–29]; the values for Tb are 218 K and 230 K [30], respectively. Gd is paramagnetic above 293 K and ferromagnetic below this temperature [29, 31]. The magnetic moment for the elements iron (Fe), cobalt (Co) and nickel (Ni) is induced by the conduction band 3d electrons and all three elements are ferromagnetic in the temperature range where measurements are performed.

For the following analysis of the magnetic layer systems we model the layer as an infinite sheet and use equations (1) and (2) to obtain the magnetic properties.

Figure 2(a) shows the f–H curve of a cantilever with a Dy (33 nm) film at room temperature. Dy is in the paramagnetic phase and no hysteresis is observed. From the curve fit we get a paramagnetic volume susceptibility of $\chi = 0.109$. This value is about 50% above the literature value [32] of $\chi = 0.0648$ in the SI system. The error lies within the uncertainties of the cantilever parameters and magnetic layer properties—in particular, the thickness of the layer. The frequency response of a cantilever with a Gd (40 nm) film in the paramagnetic and ferromagnetic phases is illustrated in figure 2(b). The Curie temperature, estimated from the transition from parabolic to non-parabolic behavior of the f–H curves, is in good agreement with the literature value of $T_c = 293$ K [29]. For temperatures around and above Curie temperature the characteristics of the frequency shifts (gray and green lines) are parabolic, indicating that the Gd film is in the paramagnetic phase. Below the Curie temperature the additional anisotropies increase and thereby intensify the frequency shift curves (red and blue lines), that are no longer parabolic in shape.

Figure 2(c) shows the frequency response of a soft magnetic Co (2.5 nm) coated cantilever with coercive field $\mu_0 H_c = 5$ mT, a saturation magnetization of $\mu_0 M_s = 0.7$ T and an anisotropy constant $K = 0.15$ MJ m^{-3} at room temperature. The saturation magnetization depends on the sample dimensions and is reduced for small particles and thin films from the value of 1.8 T for Co reported in the literature [29, 32, 33]. Figure 2(d) presents the frequency response of a hard magnetic Tb (10 nm) layer at $T = 77$ K with a coercive field of $\mu_0 H_c = 0.46$ T, saturation magnetization of $\mu_0 M_s = 0.65$ T and an anisotropy constant of $K = 0.8$ MJ m^{-3}. The cantilever is zero-field cooled (ZFC) to 77 K. The Tb layer is initially unmagnetized and is then magnetized to its saturation magnetization by applying the external field (red line). Reversing the field continuously rotates the direction of magnetization (green line). Reversing the field direction again yields a symmetric behavior (gray line). A Dy (22 nm) layer at a temperature of 5 K demonstrates as well hard magnetic behavior. Figure 2(e) illustrates the corresponding measurement yielding a coercive field of $\mu_0 H_c = 0.8$ T and an anisotropy constant of $K = 3.8$ MJ m^{-3}. The saturation magnetization amounts to $\mu_0 M_s = 0.4$ T. A $SmCo_5$ (20 nm) layer behaves like a soft magnet with a coercive field of $\mu_0 H_c = 15$ mT, a saturation magnetization of $\mu_0 M_s = 0.2$ T and an anisotropy constant of $K = 36$ kJ m^{-3} at a temperature of 77 K in figure 2(f).

The magnetization temperature dependence for the rare earth elements (Gd, Dy and Tb) in the range of 77–250 K is presented in figure 3. On decreasing the temperature the magnetization increases for all three elements. Gd is in the ferromagnetic phase in the entire temperature range and the increase of the magnetization is continuous and almost linear. In the upper temperature range, Dy is paramagnetic and the magnetization is negligible. At a temperature below 180 K, corresponding to the Néel temperature, an increase of magnetization is observed. The Curie and Néel temperatures of Tb, nearly equal, are also identified by a continuous increase in magnetization below 230 K. To calculate the magnetization, equation (2) is expanded for small magnetic moments and the magnetization is evaluated from the frequency shift. Measurements are performed without and with a magnetic field (0.73 T) and the values are subtracted to eliminate the cantilever's eigenfrequency temperature dependence [23].

To demonstrate the high sensitivity of cantilever magnetometry we perform experiments on systems with small magnetic moments. Dy is evaporated at the free end of a highly sensitive cantilever. The thickness of the Dy film is 12 nm and the volume is 0.34 am^3. The calculated magnetic moment is presented in figure 4(a). The gray points in the graph show the magnetic moment calculated for each measuring point, whereas the red line shows the calculation of the magnetic moment for a polynomial fit of the frequency response. The cantilever is zero-field cooled (ZFC) from room temperature to the temperature of liquid nitrogen, which is below the Curie temperature of Dy. The Dy film is magnetized to the saturation magnetic moment of $m = 95$ fA m^2, corresponding to 10^{10} μ_B (Bohr magnetons)[8]. Inverting the external magnetic fields yields a hysteresis loop with a coercive field of $\mu_0 H_c = 0.35$ T and a remanence ratio of 80%. Fitting the f–H curve yields an anisotropy constant of $K = 8$ MJ m^{-3}. The continuous behavior of the hysteresis loop indicates a

[7] Bruker magnet B-E-10.

[8] 10^{-15} A m^2 = 10^{-12} emu.

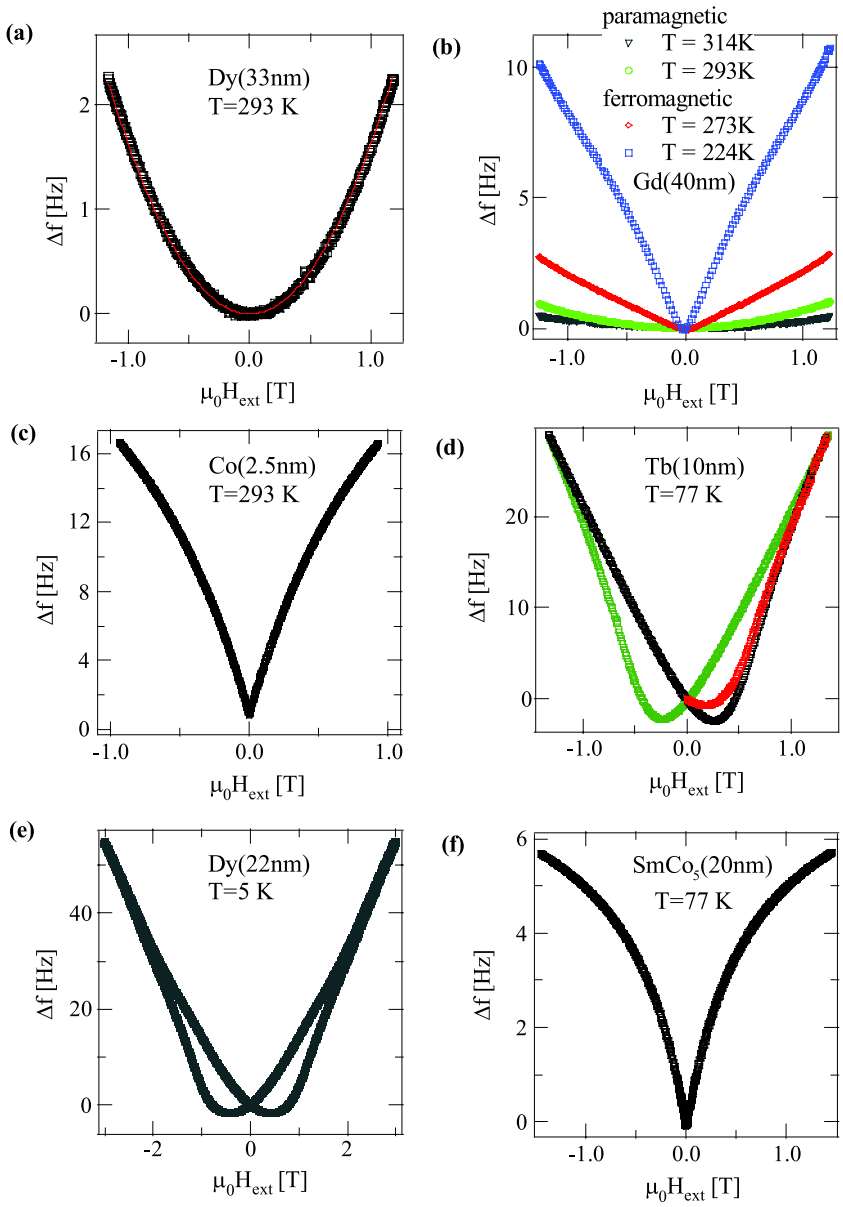

Figure 2. Measured frequency shifts of miscellaneous magnetic layer systems. (a) A Dy (33 nm) film at room temperature, where Dy is in the paramagnetic phase, is presented. The predicted parabolic shape for H_{ext} is reliably observed. Fitting the curve yields a volume susceptibility of $\chi = 0.109$. (b) Measured results for a Gd (40 nm) film at different temperatures close to the Curie temperature of 293 K. The magnetic phase transition is manifested in a change of the shape of the f–H curves. (c) A soft magnetic Co (2.5 nm) layer at room temperature is presented. (d) A hard magnetic Tb (10 nm) layer at 77 K, i.e. the Tb is in the ferromagnetic phase, is presented. The film is zero-field cooled (ZFC) and initially demagnetized. By applying a field, the layer is magnetized to its saturation magnetization (red line). Reversing the field continuously turns the direction of magnetization (green line). Reversing the field direction again yields a symmetric behavior (gray line). (e) A Dy (22 nm) layer in the ferromagnetic phase produces a coercive field of 0.8 T at 5 K. (f) A soft magnetic $SmCo_5$ (20 nm) layer is measured at 77 K.

multi-domain structure of the ferromagnetic film. In the case of a single domain or a coherent switching behavior, a quadrilateral shape is expected for in-plane hysteresis measurements. Near saturation, the magnetization process is dominated by rotation of the domains, where near the coercive field the change of magnetization is caused by domain wall motion [34–36]. A satisfactory theoretical understanding of the reversal mechanism in magnetic materials is not yet achieved [37].

In figure 4(b) a sub-micrometer sized $SmCo_5$ particle is glued at the end of a custom designed cantilever. The magnet is milled using a focused ion beam (FIB) technique to the designated shape. After milling, the magnet has a volume of 0.3 am^3. The dimensions are given in the figure. The $SmCo_5$ particle has a high coercive field of $\mu_0 H_c = 2.2$ T and a saturation magnetization of $\mu_0 M_s = 0.6$ T, according to a magnetic moment of $m = 145$ fA m^2. The anisotropy constant amounts to $K = 7.2$ MJ m^{-3}. The

Table 2. Magnetic properties of different ferromagnetic systems obtained by cantilever magnetometry.

Material thickness d (nm)	Temperature T (K)	Saturation magnetization $\mu_0 M_s (T \mathrel{\hat{=}} \mu_B/\text{atom})$	Coercive field $\mu_0 H_c$ (T)	Anisotropy constant K (MJ m^{-3})
Dy(22 ± 4.4)	5	$0.41 \pm 0.04 \mathrel{\hat{=}} 1.09 \pm 0.11$	0.8 ± 0.02	3.8 ± 1.9
Gd(40 ± 8)	77	$0.34 \pm 0.034 \mathrel{\hat{=}} 0.97 \pm 0.097$	0.07 ± 0.01	0.7 ± 0.35
Tb(10 ± 2)	77	$0.65 \pm 0.065 \mathrel{\hat{=}} 1.76 \pm 0.18$	0.46 ± 0.02	0.8 ± 0.4
Fe(14 ± 2.8)	293	$1.57 \pm 0.157 \mathrel{\hat{=}} 1.59 \pm 0.159$	0.015 ± 0.005	0.027 ± 0.014
Co(2.5 ± 0.5)	293	$0.72 \pm 0.072 \mathrel{\hat{=}} 0.67 \pm 0.067$	0.005 ± 0.002	0.15 ± 0.075
Ni(9 ± 1.8)	293	$0.23 \pm 0.023 \mathrel{\hat{=}} 0.21 \pm 0.021$	0.017 ± 0.005	0.007 ± 0.004
$SmCo_5$ (20 ± 4)	77	$0.20 \pm 0.02 \mathrel{\hat{=}} 1.49 \pm 0.149$	0.015 ± 0.005	0.036 ± 0.018
$SmCo_5$ particle	5	$0.61 \pm 0.061 \mathrel{\hat{=}} 4.58 \pm 0.458$	2.2 ± 0.01	7.2 ± 3.6

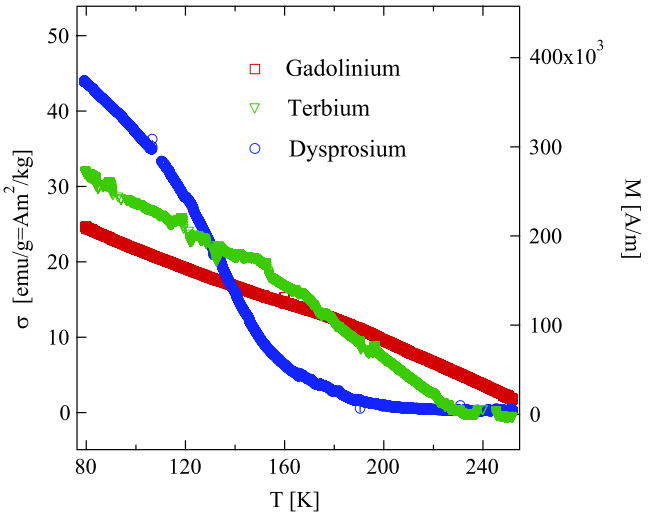

Figure 3. Magnetization of the rare earth elements Gd, Tb and Dy in the temperature range $T = 77$–250 K. Gd is ferromagnetic and has a continuous increase of magnetization on decreasing the temperature, whereas Dy is paramagnetic in the upper temperature range and the magnetization is negligible. Below 180 K, according to the Néel temperature of Dy, the magnetization increases for lower temperatures. Tb shows the same behavior as Dy for a temperature of 230 K.

magnetic properties obtained are equal for modeling the magnetic particle as a sphere and as a rod, indicating that the magnetocrystalline anisotropy constant dominates the shape of the f–H curve. Again the saturation magnetization for nanometer sized samples is diminished from the value of 1 T for macroscopic samples [38, 39]. The presence of domains indicates coherent switching behavior.

Magnetotactic bacteria, such as *Magnetospirillum gryphiswaldense bacteria* [40], incorporate chains of single-crystalline magnetite Fe_3O_4 particles with diameters of about 30 nm. The linear magnetite chain, called the magnetosome, is made of approximately 18 dipoles which are enclosed by a membrane to prevent an agglutination of the magnetic particles. The bacteria use the magnetosome as a compass needle, for their spatial orientation in water. Cantilever magnetometry with an ensemble of randomly oriented protozoa using a commercially available sensor[9] at room temperature is presented in figure 4(c). The coercive field measures 20 mT. The absence of an initial magnetization curve in the first measurement proves that the magnetosomes are initially in the saturated state. The size of the magnetic particle is above the superparamagnetic limit and we assume that each magnetic sphere is a single-domain particle. A measurement of about 100 protozoa yields an average magnetic moment of 5×10^{-16} A m^2 for each of the protozoa. The magnetic properties are in good agreement with results obtained from electron holography measurements [41].

Table 2 summarizes the magnetic properties of the ferromagnetic systems analyzed. The saturation magnetization and the anisotropy constant are obtained by fitting the measured f–H curves for saturation with equation (2). The coercive field is the magnetic field at which the frequency equals the zero-field frequency after magnetic reversal and is extracted from the f–H curves.

In order to estimate the accuracy of the values in table 2 we fitted the data several times with different initial parameters. The values of the saturation magnetization lie within an error of about 10%. For the values of the anisotropy constant the accuracy is unfortunately not better than 50%. To obtain more accurate values of the anisotropy constant, cantilever magnetometry should be performed at higher magnetic fields where the shape of the f–H curve is strongly influenced by the anisotropy constant. The values obtained for the saturation magnetization are below the values for macroscopic ferromagnetic systems reported in the literature [32, 33].

5. Conclusions and outlook

Cantilever magnetometry is a powerful tool for the analysis of nanomagnetic systems. It is found that the frequency shift of the cantilever depending on the applied magnetic field provides a convenient method for determining the magnetic properties. Adequate models are developed for quantifying the results. Magnetic moments, as small as 10^{10} μ_B (Bohr magnetons), were detected and the resolution is estimated to be 10^7 μ_B. Paramagnetic thin films were used to verify the theoretical models. Values of the susceptibility of the thin films of Dy in the paramagnetic phase are in agreement with the literature values with an accuracy of 50%. Temperature dependences of thin films made of lanthanoids, such as Gd, Dy and Tb, were investigated. In the case of Gd the transition from the paramagnetic to the ferromagnetic temperatures is observed

[9] ARROW-TL1-50, Tipless Silicon-SPM-Sensor, www.nanoworld.com.

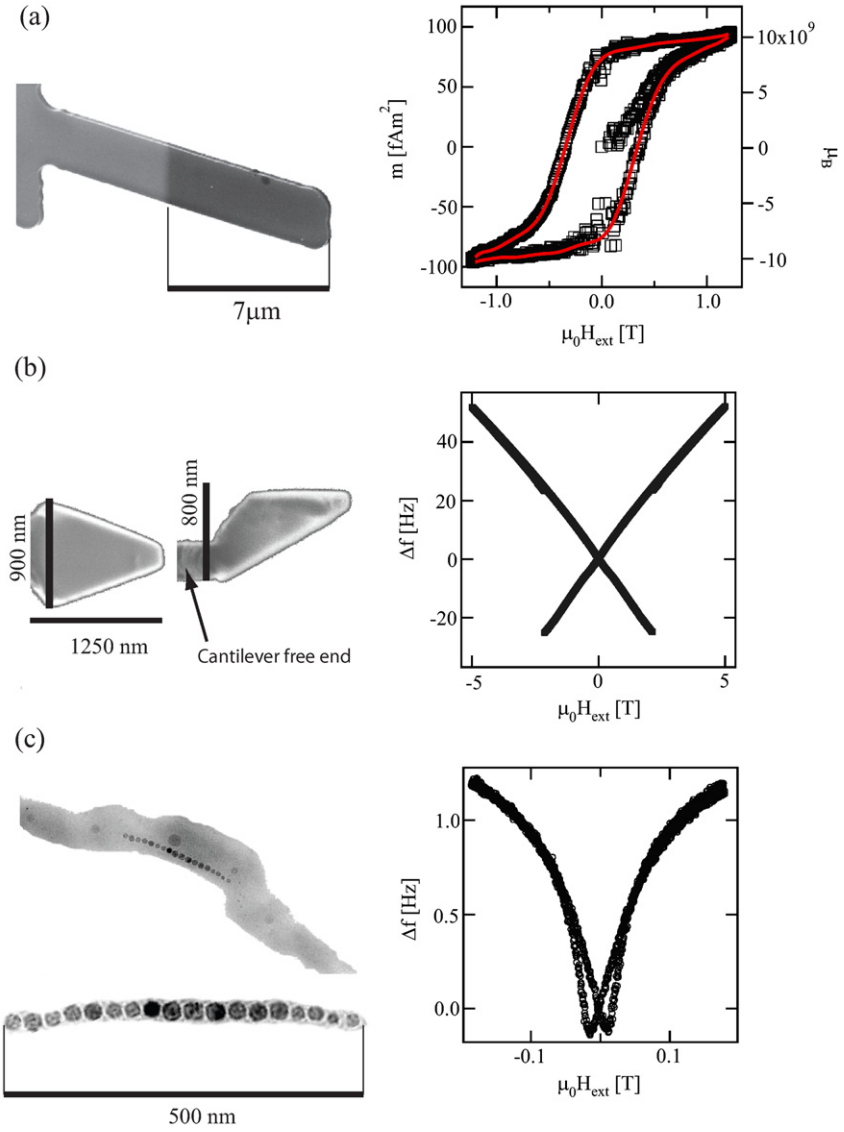

Figure 4. (a) A hysteresis loop of a cantilever with a 12 nm thick Dy layer in the ferromagnetic phase at a temperature of 77 K is presented. After zero-field cooling (ZFC) the Dy layer is magnetized to its saturation magnetization of $m = 95$ fA m^2. Reversing the applied field yields a symmetric hysteresis loop. The magnetic moment is calculated from the frequency shift of the cantilever. (b) A nanometer sized $SmCo_5$ particle is presented. The particle is shaped using the FIB technique and shows high coercivity of 2.2 T at a temperature of 5 K and a saturation magnetization of 0.6 T. (c) An f–H curve for a cantilever with magnetotactic bacteria at room temperature is measured. The coercive field is 20 mT. The absence of an initial magnetization curve in the hysteresis loop indicates that the ferromagnetic domains of the sample are initially not randomly oriented. The image on the left side shows a transmission electron micrograph (TEM) image of a magnetosome with a chain of magnetic nanoparticles about 30 nm in diameter incorporated in the *Magnetospirillum gryphiswaldense bacteria*.

at the correct Curie temperature. Furthermore, measurements were made on soft and hard ferromagnetic thin films of Co and Tb, and hard magnetic particles, such as $SmCo_5$. The corresponding f–H curves give insight into the mechanisms of magnetization and magnetic reversal of these films and particles. The saturation magnetization is assigned within an accuracy of 10% from fitting the measured data. The anisotropy constants have uncertainties of 50%.

Reducing the dimensions, especially the thickness, of the micromechanical sensors will further improve the sensitivity by an order of magnitude. Under these conditions, a single bacterium or individual nanoparticles with magnetic moments of 10^2–10^3 μ_B may become accessible to magnetometry.

Acknowledgments

The following persons made this work possible by providing samples and cantilevers: Dong Weon Lee, Jiandong Wei and Sara Romer. We thank Hans Peter Lang for final corrections. This work was supported by the Swiss National Foundation and the National Center of Competence in Research on Nanoscale Science.

References

[1] Bader S D 2006 *Rev. Mod. Phys.* **78** 1
[2] Grundy P J 1998 *J. Phys. D: Appl. Phys.* **31** 2975–90

[3] Gregg J F, Petej I, Jouguelet E and Dennis C 2002 *J. Phys. D: Appl. Phys.* **35** R121–55
[4] Pankhurst Q A, Connolly J, Jones S K and Dobson J 2003 *J. Phys. D: Appl. Phys.* **36** R167–81
[5] Brown W F Jr 1963 *Micromagnetics* (New York: Wiley)
[6] Binnig G, Quate C F and Gerber Ch 1986 *Phys. Rev. Lett.* **56** 930
[7] Marohn J A, Fainchtein R and Smith D D 1998 *Appl. Phys. Lett.* **73** 3778
[8] Moreland J 2003 *J. Phys. D: Appl. Phys.* **36** R39–51
[9] Stipe B C, Mamin H J, Stowe T D, Kenny T W and Rugar D 2001 *Phys. Rev. Lett.* **86** 2874
[10] Nga Ng T, Jenkins N E and Marohn J A 2006 *IEEE Trans. Magn.* **42** 378–81
[11] Stoner E C and Wohlfarth E P 1948 *Phil. Trans. R. Soc.* **240** 599–642
[12] Martin Y and Wickramasinghe H K 1987 *Appl. Phys. Lett.* **50** 1455
[13] Sàenz J J *et al* 1987 *J. Appl. Phys.* **62** 4293
[14] Landau L D, Lifshitz E M and Pitaevskii L P 1995 *Electrodynamics of Continuous Media* (Oxford: Heinemann Butterworth)
[15] Sidles J A, Garbini J B, Bruland K J, Rugar D, Zueger O, Hoen S and Yannoni C S 1995 *Rev. Mod. Phys.* **67** 249
[16] Slepyan G Y, Maksimenko S A, Hoffmann A and Bimberg D 2002 *Phys. Rev.* A **66** 063804
[17] How H and Vittoria C 1991 *Phys. Rev.* B **43** 8094–104
[18] Johnson M T, Bloemen P J H, den Broeder F J A and de Vries J J 1996 *Rep. Prog. Phys.* **59** 1409–58
[19] Giessibl F J 2003 *Rev. Mod. Phys.* **75** 949–83
[20] Rast S, Gysin U and Meyer E 2009 *Phys. Rev.* B **79** 054106
[21] Albrecht T R, Grütter P, Home D and Rugar D 1991 *J. Appl. Phys.* **69** 668
[22] Lee D W, Kang J, Gysin U, Rast S, Meyer E, Despont M and Gerber C 2005 *J. Micromech. Microeng.* **15** 2179–83
[23] Gysin U, Rast S, Ruff P, Meyer E, Lee D W, Vettiger P and Gerber C 2004 *Phys. Rev.* B **69** 045403
[24] Werle C 2007 *Master Thesis* NW Fachhochschule Nordwestschweiz, Institute for Microelectronics
[25] Gysin U, Rast S, Kisiel M, Werle C and Meyer E 2011 *Rev. Sci. Instrum.* **82** 023705
[26] Meyer G and Amer N M 1988 *Appl. Phys. Lett.* **53** 2400–2
[27] Behrendt D R, Legvold S and Spedding F H 1958 *Phys. Rev.* **109** 1544
[28] Elliott R J 1961 *Phys. Rev.* **124** 346–53
[29] Ashcroft N M and Mermin N D 1976 *Solid State Physics* (Philadelphia, PA: Saunders)
[30] Thoburn W C, Legvold S and Spedding F H 1958 *Phys. Rev.* **112** 56–8
[31] Elliott J F, Legvold S and Spedding F H 1953 *Phys. Rev.* **91** 28
[32] 1999–2000 *Handbook of Chemistry and Physics* 80th edn (Boca Raton, FL: CRC Press) pp 4–131
[33] O'Handley R C 2000 *Modern Magnetic Materials* (New York: Wiley)
[34] Kittel C 1949 *Rev. Mod. Phys.* **21** 541–83
[35] Stoner E C 1953 *Rev. Mod. Phys.* **25** 2–16
[36] Brown W F 1945 *Rev. Mod. Phys.* **17** 15
[37] Aharoni A 2001 *Physica* B **306** 1
[38] Benz M G and Martin D L 1970 *Appl. Phys. Lett.* **17** 176
[39] Foner S, McNiff E J, Martin D L and Benz M G 1972 *Appl. Phys. Lett.* **20** 447
[40] Blakemore R P 1975 *Science* **190** 377–9
[41] Dunin-Borkowski R E, McCartney M R, Frankel R B, Bazylinski D A, Pòsfai M and Buseck P R 1998 *Science* **282** 1868–70